

Link to original published version: <http://dx.doi.org/10.1016/j.desal.2014.04.016>

Citation: Barello M, Manca D, Patel R and Mujtaba IM (2014) Neural network based correlation for estimating water permeability constant in RO desalination process under fouling. *Desalination*. 345: 101-111.

Copyright statement: © 2014 Elsevier B.V. Full-text reproduced in accordance with the publisher's self-archiving policy.

This manuscript version is made available under the CC-BY-NC-ND 4.0 license
<http://creativecommons.org/licenses/by-nc-nd/4.0/>



**Neural network based correlation for estimating water permeability constant in
RO desalination process under fouling**

M. Barello*, D. Manca*, R. Patel**, I.M. Mujtaba**

**Dipartimento di Chimica Industriale e Ingegneria Chimica "G. Natta", Politecnico di Milano
Piazza Leonardo da Vinci 32, 20133 Milan, Italy.*

***Chemical Engineering Division, School of Engineering, University of Bradford
West Yorkshire BD7 1DP, UK I.M.Mujtaba@bradford.ac.uk*

Abstract

The water permeability constant, (K_w) is one of many important parameters that affect optimal design and operation of RO processes. In model based studies, e.g. within the RO process model, estimation of K_w is therefore important. There are only two available literature correlations for calculating the dynamic K_w values. However, each of them are only applicable for a given membrane type, given feed salinity over a certain operating pressure range. In this work, we develop a time dependent neural network (NN) based correlation to predict K_w in RO desalination processes under fouling conditions. It is found that the NN based correlation can predict the K_w values very closely to those obtained by the existing correlations for the same membrane type, operating pressure range and feed salinity. However, the novel feature of this correlation is that it is able to predict K_w values for any of the two membrane types and for any operating pressure and any feed salinity within a wide range. In addition, for the first time the effect of feed salinity on K_w values at low pressure operation is reported. While developing the correlation, the effect of numbers of hidden layers and neurons in each layer and the transfer functions is also investigated.

Keywords: Reverse Osmosis, Physical property models; Fouling; Water permeability elevation; Neural networks modelling.

1. Introduction

1.1. RO desalination

Desalination of both sea and ground waters has been utilized for water supply throughout the world for over 40 years. The two most widely used desalination techniques are reverse osmosis (RO) and multi-stage flash (MSF) distillation. The RO separation process for water desalination has some advantages in terms of energy saving, modularity, flexibility and ability to construct small size plants with even less installation space in comparison to MSF [1,2]. Although progress has been made in

various aspects of their application, the issue of fouling remains a major operational problem which results in additional capital, labour, chemical and energy costs to the industry [3,4]. These costs arise due to the loss of membrane performance (permeability) over time and the subsequent need for cleaning or replacing fouled units. The importance of the water permeability constant (K_w) can be clearly seen from the mass balance equation (1):

$$J_w = K_w (\Delta P - \Delta \pi) \quad (1)$$

where J_w is the water flux through the membrane, and ΔP the pressure difference between the feed and permeate sides of the membrane. Similarly, $\Delta \pi$ is the osmotic pressure difference across the membrane. It can be seen that a decay in the water permeability constant (K_w) results in a lower J_w values and consequently, in worse plant performance.

1.2. Membrane fouling and mechanism

At the beginning, some attention should be paid to the definition of the term “membrane fouling”, which appears very often in the literature discussing water and wastewater treatment by membrane methods. Normally, the phenomenon is characterised by a long term flux decline and, eventually, retention decrease as a result of accumulation of some fouling material. Fouling may be caused by several compounds and these foulants may be classified as [5]:

- dissolved organics, including humic substances, biological slimes and macromolecules;
- dissolved inorganics, including inorganic precipitates such as CaSO_4 , CaCO_3 , Mg(OH)_2 , Fe(OH)_3 , and other metal hydroxides;
- particulate matter.

Jackson and Landolt [6] studied the rate of fouling by deposition of iron hydroxide on tubular RO membranes. They found that the fouling occurred via a two-step-growth mechanism. This fouling mechanism may be applicable to other foulants as well. Initially, in the nucleation phase, foulants are deposited in pores and surface holes of the membrane. This occurs because of the mechanical force acting from the convective flow foulants to the membrane surface and *Van der Waals'* force of attraction. The relative size of the foulant, the number of pores in the membrane and surface charges affect the number of nucleation sites. The second step in the growing mechanism starts when sufficient foulants are trapped on the membrane surface, and they can act as nuclei from which growth

proceeds by a polymerization reaction. Large fouling particles build up on the membrane surface forming a thin porous layer. The rate of growth of this layer depends on the nuclei concentration, the rate of polymerization reaction and the rate of transport of foulants to the membrane surface.

Gregor and Gregor [7] explain that fouling is normally caused by materials that have large surface area and are hydrophobic. When a hydrophobic substance is in an aqueous solution, the total dissolution energy can be reduced by decreasing the area exposed to the water. Therefore, this substance would adhere to the membrane surface by eliminating the repulsive interactions with the surrounding water. Fouling materials normally have a negative charge due to hydrogen bonding and this will further increase the fouling phenomenon.

Jonsson and Kristen [8] distinguished between different types of fouling: irreversible adsorption of hydrophobic substances to the membrane surface and reversible sorption of different compounds within the membrane phase. The former depends mainly on the transport of foulants to the membrane surface, influenced by the concentration in the bulk solution and the total permeate volume. Therefore, it depends strongly on the elapsed time and the membrane hydrodynamics. Further, membranes require either mechanical or chemical cleaning in order to restore the pure water permeability. The reversible sorption mechanism results in smaller K_w values compared with water, because of increased frictional resistance and a decrease in the water content of the membrane. Due to the existence of dynamic equilibrium between the bulk solution and the membrane phase, the change in K_w is sudden and there is no time dependency as above.

Water permeability constant is not only a function of the operating time, but it also depends on the membrane type (*i.e.* spiral wounds, hollow fibre, tubular) [9], on the water quality (salinity) [10] and on the operating pressure [11].

1.3. Fouling correlations

Only two correlations in the literature [11 and 12], used to calculating K_w for RO processes under fouling have been developed previously and are listed in Table 1 with some specific details. These correlations take into consideration only the effect of fouling with time, and they are applicable for the respective membrane type only and for very specific values of pressure and feed salinity. It places limitation on such correlations, because the salt concentration in seawater around the world varies

markedly. Figure 1 shows the K_w estimated profiles given by the two correlations. As it is possible to see, the trend is progressively decreasing with the time, due to the fact that both correlations consider the fouling influence.

Therefore, it is worth developing a correlation which acts over a wide range of operating parameters and still consider the dynamic evolution of the fouling phenomenon, which can be confidently used for modelling, simulation, and optimisation of RO processes.

The use of neural networks (NNs), in all aspects of process engineering activities, such as modelling, design, optimisation, and control, has considerably increased in recent years [13, 14, 15].

In this work, a time dependant NN based correlation is developed for estimating K_w for any salinity and operating pressure under fouling, considering two membrane types: hollow fiber [11] and spiral wound [12]. The ultimate objective is to use this correlation within a RO process modelling and optimisation framework in future. In addition, the NN architecture is characterised by studying the influence of number of hidden layers and neurons for each layer. Eventually, the role of the transfer function on the NN performance is investigated.

2. Neural network based correlation

Artificial neural networks are inspired by the architecture of biological nervous system which consists basically of a large combination of simple nerve cells or neurons that work in parallel to facilitate rapid decisions. Analogously, NNs are made up of a large number of primitive computational elements that are organised in a massive parallel set. The NN is then developed in artificial synapses that connect these elements, which are characterised by a set of weights, which can typically be adjusted by a learning process. The most important advantage in using this mathematical method, is that NNs do not have to be programmed, instead they use examples to learn how to deal with more complex relationships.

NNs have proved to be highly successful in applications such as process control, modelling, simulation and system identification [16, 17, 18]. Their popularity could be attributed to the fact that NNs can solve many different types of engineering problems with a relatively simple and flexible structure, due to their superior calculating ability.

In essence, neural networks consist of networks of primitive elements (neurons) that receive signals (inputs) from other neurons or from the outside. These signals are subsequently weighted and

summed. The results (also called potentials of the neurons) are then computed by transfer functions, which pass the output to other nodes to the outside environment of the network. The network has a structure consisting of at least an input and an output layer, and possibly one or more hidden layers. Neurons in these layers are connected by means of artificial synapses, each of which is associated with a numerical value or weight. Once the NN is built, trained, validated and tested, with respect to a different set of inputs, it is able to produce a corresponding set of outputs according to the inner mapped relationship. This relationship depends upon the parameters of the network, *i.e.* the optimal set of weights and biases [19].

2.1 NN architecture and training

A neural network architecture design depends on the number of layers the network has, the number of neurons in each layer, the transfer function used in each layer, and how the layers are connected to each other. A typical NN architecture is shown in Figure 2.

Each neuron, j , in the i -th layer is fed by a dedicated bias (b_j^i) and is connected with the neurons of the $(i-1)$ -th layer (except the input layer) through the weights (w_{jk}^i). k denotes the neuron of $(i-1)$ -th layer. The total number of neurons in layer i is n_j and the transfer function for layer i and neuron j is f_j^i . In each layer, the value of the neuron a_j^i is then calculated as follows:

$$a_j^i = f_j^i \left(\sum_{k=1}^{n_{i-1}} w_{jk}^i \times a_k^{i-1} + b_j^i \right) \quad (2)$$

In this work, the Levenberg-Marquardt back propagation algorithm is used to train the network [19]. Despite the fact that it requires more memory space and does not converge quickly like other algorithms, it is characterised by better performances because it gets closer to the optimal solution. An appropriately trained and validated network should be able to predict realistic outputs even when the network is presented with new inputs (test data).

Although neural networks are able to interpolate data very well, they are not quite efficient with extrapolation [19]. That is why it is very important to choose an appropriate interval for the inputs value. In order to ensure that the NN gives good results, a large number of data set is usually required during the training session. In this work, the training data set is selected in such a way that it includes

the data from all regions of a desirable simulation. The calculations continue until the error between the predicted and target value is close to zero (Figure 3).

2.2 Development of correlations

The correlation estimates K_w in terms of time (t), salinity (x_f), operating pressure (P) and membrane type (M). K_w is expressed in [m/bar/min], x_f expressed in [g/l] and P expressed in [bar].

The input data are scaled up by the mean and their standard deviation values are as follows:

$$t_{scaleup} = \frac{t - t_{mean}}{t_{std}} \quad (3)$$

$$x_{scaleup} = \frac{x_f - x_{f_{mean}}}{x_{f_{std}}} \quad (4)$$

$$x_{scaleup} = \frac{x_f - x_{f_{mean}}}{x_{f_{std}}} \quad (5)$$

$$M_{scaleup} = \frac{M - M_{mean}}{M_{std}} \quad (6)$$

where t_{mean} is the average of t , $x_{f_{mean}}$ the average of x_f , P_{mean} the average of P and M_{mean} the average of M ; t_{std} is standard deviation of t , $x_{f_{std}}$ the standard deviation of x_f , P_{std} the standard deviation of P and M_{std} the standard deviation of M data used to develop the correlation.

There are four input neurons in the NN based correlations and the values are:

$$a_{1\ scaleup}^1 = t \quad ; \quad a_{2\ f_{scaleup}}^1 = x_f \quad ; \quad a_{3\ scaleup}^1 = P \quad ; \quad a_{4\ scaleup}^1 = M$$

There is one output neuron in the NN based correlations:

$$a_j^l = K_{w_{scaleup}} \quad (7)$$

where l is the output layer.

The output value is rescaled to find the value in original units by the following equation.

$$K_w = K_{w_{scaleup}} \times K_{w_{std}} + K_{w_{mean}} \quad (8)$$

For a network as shown in Figure 2, the correlation for the output is given by:

$$a_1^3 = f_1^3 \left(\sum_{k=1}^4 (w_{1k}^3 a_k^2) + b_1^3 \right) \quad (9)$$

where the outputs from the second layer (a_k^2) are given by:

$$a_k^2 = f_j^2 \left(\sum_{k=1}^2 (w_{jk}^2 a_k^1) + b_j^2 \right) \quad (10)$$

For $j=1$ (first neuron) in layer 2, Eq. (9) can be expressed as:

$$a_1^2 = f_1^2 (w_{11}^2 a_1^1 + w_{12}^2 a_2^1 + b_1^2) \quad (11)$$

In this work, transfer functions $f^2 = \tanh$ and $f^3 = 1$ are initially applied, and the influence of this choice on the network's performances is investigated later in this paper. Equation (11) thus becomes:

$$a_1^2 = \tanh(w_{11}^2 f_{scaleup} + w_{12}^2 x_{f_{scaleup}} + w_{13}^2 P_{scaleup} + w_{14}^2 M_{scaleup} + b_1^2) \quad (12)$$

The output that the network returns is:

$$K_{w_{scaleup}} = a_1^3 = w_{11}^3 a_1^2 + w_{12}^3 a_2^2 + w_{13}^3 a_3^2 + w_{14}^3 a_4^2 + b_1^3 \quad (13)$$

3 Data used

The input data for the NN are generated using the two existing correlations published in the literature [11] and [12]. Zhu *et al.* [11] studied a systematic technique for the optimal design and scheduling of flexible osmosis networks that can accommodate a given range of potential variations in the characteristics of the feed and system performance (varying permeability caused by fouling). They considered a hollow fibre membrane, a feed concentration of 34.80 [g/l], pressure in the range 62-70 [atm] and operating time 370 days. The exponential correlation they used for describing the water permeability decay was however not validated with any experimental data.

Al-Bastaki and Abbas [12] looked at the long term performance of a medium scale industrial reverse osmosis water desalination plant with a spiral wound membrane. They used a feed concentration of 25.40 [g/l], an operating pressure of 12 [bar] and studied the performances over a period of 1500 days. Their correlation was proposed based on experimental data.

In order to develop the NN based correlation, we have generated 370 days of data which are considered for training and validating and testing the correlation. The data set considered in this work

corresponds to 372 points where for each time value there are two pressures, two feed salinities and two membrane types (Table 3).

From all the input data shown in Table 3, the first two points are selected for training (bold), the next input data point for validation (italic) and the fourth one for testing (normal) the correlations. This selection process continues sequentially until all the data points are exhausted. Thus, the total input data are divided into three data sets: training (50%), validation (25%) and testing (25%). The training values are used to adjust the network based on the error, and the validation data are used to measure network generalization and to halt training when generalization stop improving. The test data do not have any effect on training thus providing an independent measure of network performance during and after training.

As a base case, one hidden layer with four neurons was used in the correlation (Figure 4). Also, a hyperbolic tangent function and a linear function were adopted between the input and hidden layer and between the hidden and output layer.

4 Results

With reference to Figure 4, the NN based correlation can be expressed as follows.

The values for the hidden layer neurons are:

$$\alpha_1^2 = \tanh \left(w_{11}^2 t_{scaleup} + w_{12}^2 x_{f_{scaleup}} + w_{13}^2 P_{scaleup} + w_{14}^2 M_{scaleup} + b_1^2 \right) \quad (14)$$

$$\alpha_2^2 = \tanh \left(w_{21}^2 t_{scaleup} + w_{22}^2 x_{f_{scaleup}} + w_{23}^2 P_{scaleup} + w_{24}^2 M_{scaleup} + b_2^2 \right) \quad (15)$$

$$\alpha_3^2 = \tanh \left(w_{31}^2 t_{scaleup} + w_{32}^2 x_{f_{scaleup}} + w_{33}^2 P_{scaleup} + w_{34}^2 M_{scaleup} + b_3^2 \right) \quad (16)$$

$$\alpha_4^2 = \tanh \left(w_{41}^2 t_{scaleup} + w_{42}^2 x_{f_{scaleup}} + w_{43}^2 P_{scaleup} + w_{44}^2 M_{scaleup} + b_4^2 \right) \quad (17)$$

and

$$K_{w_{scaleup}} = \alpha_1^3 = w_{11}^3 \alpha_1^2 + w_{12}^3 \alpha_2^2 + w_{13}^3 \alpha_3^2 + w_{14}^3 \alpha_4^2 + b_1^3 \quad (18)$$

The network is trained, validated, tested and simulated using the Matlab NN toolbox, *nntool*. The software evaluates the weight and bias values and a graphical performance assessment of the network as shown by a typical example in Figure 5. It is possible to see that in this particular case, the training took 17 iterations. The result here is reasonable, because the final mean square error is

relatively small, the test set and validation set errors have similar characteristics, and it appears that significant over-fitting has not occurred. Table 4 shows the scaled up input and target parameters whilst the weights and biases are shown in Table 5. The statistical regression between the predicted value (A) of the water permeability constant K_w from the NN correlation and correlations data (T) is plotted to find the overall trends of the predicted data. An example is shown in Figure 6. The regression plot is used to study the influence of the number of layers, number of neurons and transfer function on the NN performance. A perfect architecture would result in a regression value (R) of 1.0.

5 Discussions

Figure 7 shows the prediction of K_w by the NN based correlation and that by Al-Bastaki and Abbas [12] for $x_f=25.40$ g/L, $P=12$ bar, $M=1$. Figure 8 shows the prediction of K_w by the NN based correlation and that by Zhu et al. [11] for $x_f=34.8$ g/L, $P=66$ bar, $M=2$. The results clearly show that the predictions by NN correlations are as good as those predicted by existing correlations.

It is known [13], that NN based correlations are powerful tools for predicting interpolated data, but they are not able to generate good results if the actual inputs' range is not the same as those used for training, validating and testing the network. To illustrate this point, a test case was run for Al-Bastaki and Abbas [12] correlations for a period of 1500 days. The results are shown in Figure 9 and it is clear that the NN based correlation gives good results only up to 370 days, i.e. the upper time limit for which the network was trained. Beyond that the NN predictions and the data generated by Al-Bastaki and Abbas [12] diverge quite rapidly.

Most important contribution of this work is to be able to predict K_w for any membrane type ($M=1$ or $M=2$) for any salinity ranging from 25.4 – 34.8 g/l and any operating pressure ranging from 12-66 bar using Neural Network technique. For membrane type $M=1$ and feed salinity of 25.4 g/L (as used by Al-Bastaki and Abbas [12]), the effect of pressure on the K_w is evaluated and is shown in Figure 10. Also for membrane type $M=2$ and feed salinity of 34.8 g/L (as used by Zhu *et al* [11]), the effect of pressure on the K_w is evaluated and is shown in Figure 11. In both cases, the trend is confirmed by authors that studied the influence of the operating pressure on the water permeability constant [20]. It is observed that at lower feed salinity (Figure 10) the increase in pressure produces a greater % change in K_w towards the end of the simulation time. There is no literature evidence of this behaviour, but we anticipate that this could be due to the concentration polarization phenomenon. This phenomenon

describes the concentration gradient of salts on the high-pressure side of the reverse osmosis membrane surface created by the re-dilution of salts left behind as water permeates through the membrane itself. Its value tends to be smaller at higher feed salinity [21]. Thus, at lower feed salinity (Figure 10) the pressure influence on the K_w is more evident than at higher feed salinity (Figure 11).

For membrane type M=1 and P=12 bar (as used by Al-Bastaki and Abbas [12]), the effect of feed salinity is shown in Figure 12. Also for membrane type M=2 and P=66 bar (as used by Zhu *et al* [11]), the effect of feed salinity is shown in Figure 13. The results show a rapid decrease in K_w with increasing feed salinity in Figure 12. This dependence has often been ignored in the literature. However, at higher pressures (Figure 13) the influence of the feed salinity on the K_w trend is less evident. Since there is no evidence in the literature of this relationship, we might postulate that at higher pressures the driving force of the mechanism dominates all other parameters influences.

5.1 Effect of number of hidden layers

This section investigates the effect of the number of hidden layers on the neural network performance. Each hidden layer has four neurons as the input layer; whilst the output layer has one neuron only. The performance, shown in Table 6, is evaluated by monitoring the iteration time and the goal reached using Matlab. The respective regressions are shown in Figure 14.

It can be seen that the predicted values for 2-, 3- and 5-layer reflect quite well the target values of the correlations data. For these architectures, although the number of iterations is increasing with the number of layers, there is an improvement in the performances. As the number of layers is increased to 10 and 20 layer, the predictions became rather inaccurate.

5.2 Effect of number of neurons

The effect of modifying the number of neurons, from 2 to 20, is now considered for a three layered network. The results from the NN simulations are shown in Figure 15 and Table 7 in accordance with the study of the number of layers. It can be seen that for all the different NN architectures the correlations and the predicted data correlate quite well. There is however some oscillatory behaviour when the number of neuron is increased.

Looking at the Matlab performances evaluations (Table 7) one can see that a 3 neurons configuration is better than 5 and 10. Also, the 20 neurons network shows a value nearer to the goal (set at 0) even though it takes longer iteration time to reach such a target.

5.3 Effect of transfer functions

The transfer functions that Matlab proposes as connections between layers are listed shown schematically in Figure 16. *Purelin* is a linear transfer function, *tansig* is a hyperbolic tangent sigmoid transfer function and *logsig* is a log-sigmoid transfer function. The differences between these transfer functions are evaluated in terms of performances for a three layered NN with four neurons in the hidden layer with the same transfer function in each layer. The results for each transfer function are shown in Figure 17 and the results for each transfer function are reported in Table 8.

It can be seen that the *tansig* function produces the best predictions for this NN architecture in terms of goal, epochs and comparison with the correlations data from the regression plotted in Figure 17.

6 Conclusions

This work develops a NN based correlation to predict the dynamic water permeability constant K_w for a RO desalination plant under fouling. A multi-layered feed-forward network trained with back propagation method has been implemented. The proposed NN model structure (with one hidden layer and four neurons in hidden layer) is capable of predicting the dynamic K_w very close to those predicted by existing correlations in the literature. Compared to existing correlations, the distinguishing feature of this correlation is that it is able to predict dynamic K_w values for any of the two membrane types used in the literature and for any operating pressure and any feed salinity within a wide range. In addition, although the effect of pressure on K_w values is in-line with those observed in the literature, this works adds another dimension to existing literature that the effect of feed salinity on K_w values can be more pronounced at low pressure operation (which was not reported in the past).

For a given architecture, the correlation can be updated with additional data from other sources or a new correlation can be developed for the new source data. The influence of some network design parameters such as numbers of hidden layer, number of neurons and chosen transfer functions are also studied. In detail, it is found that a small number of layers (2, 3 and 5) reflects quite well the target values of the data. For the internal layer structure, it is found that a 3 neurons configuration is better than 5 and 10. In matter of transfer function, the obtained results bring the conclusion that *tansig*

function gives the best predictions for this NN architecture in terms of goal, epochs and comparison with the target data.

Nomenclature

<i>A</i>	Water permeability NN value, m/bar/min
<i>a</i>	Neuron value, -
<i>b</i>	Bias, -
<i>f</i>	Transfer function, -
<i>J</i>	Flow rate, m ³ /min/m ²
<i>K</i>	Permeability constant, m/bar/min
<i>M</i>	Membrane type, -
<i>P</i>	Operating pressure, bar
<i>T</i>	Water permeability target value, m/bar/min
<i>t</i>	Time, day
<i>w</i>	Weight, -
<i>x</i>	Concentration, g/l
ΔP	Net hydraulic pressure differential across the membrane, bar
$\Delta \pi$	Net osmotic pressure differential across the membrane, bar

Subscripts

0	Initial value
<i>f</i>	Feed
<i>j</i>	Neuron
<i>k</i>	i-1
mean	Average value
scaleup	Scaled up value

std Standard deviation

W Water

Superscripts

i Layer

References

- [1] M. Schiffler, Perspectives and challenges for desalination in the 21st century, *Desalination*, 165 (2004) 1–9.
- [2] M. Kuriara, Y. Hiroyuki and N. Takayuki, High recovery/high pressure membrane for brine conversion SWRO process development and its performance, *Desalination*, 125 (1999) 9–15.
- [3] C. Whittaker, H.R. Ridgeway, B.H. Olson, Evaluation of cleaning strategies for removal of biofilms from reverse osmosis membranes, *Applied and Environmental Microbiology*, 48 (1984) 395–403.
- [4] K.M. Sassi, I.M. Mujtaba, Optimal design and operation of reverse osmosis desalination process with membrane fouling, *Chemical Engineering Journal*, 171 (2011) 582-593.
- [5] G. Belfort, G. Alexandrovics, B. Marx, Artificial particulate fouling of hyperfiltration membranes, *Desalination* 19 (1976) 127-138.
- [6] J.M. Jackson, D. Landolt, About the mechanism of formation of iron hydroxide fouling layers on reverse osmosis membranes, *Desalination* 12 (1973) 361-378.
- [7] H.P. Gregor, C.D. Gregor, Synthetic membrane technology, *Scientific American*, 239 (1978) 88-101.
- [8] G. Jonsson, S. Kristen, Membrane filtration of NSSC-waste liquor, *Desalination* 32 (1980) 327-339.
- [9] F. Evangelista, A short cut method for the design of reverse osmosis desalination plants, *Industrial and Engineering Process Design and Development*, 24 (1985) 221-223.
- [10] M. Wilf, K. Klinko, Performances of commercial seawater membranes, *Desalination*, 96 (1994) 465-478.
- [11] M. Zhu, M.M. El-Halwagi, M. Al-Ahmad, Optimal design and scheduling of flexible reverse osmosis networks, *Journal of Membrane Science*, 129 (1997) 162-174.
- [12] N. Al-Bastaki, A. Abbas, Long-term performance of an industrial water desalination plant, *Chemical Engineering Processing*, 43 (2004) 555-558.

- [13] I.M. Mujtaba, M.A. Hussain, Application of Neural Network and Other Learning Technologies in Process Engineering. London, Imperial College Press, 2001.
- [14] M.S. Tanvir, I.M. Mujtaba, Neural Network based correlations for estimating temperature elevation for seawater in MSF desalination process, *Desalination* 195 (2006) 251-272.
- [15] A. Aminian, Prediction of temperature elevation for seawater in multi-stage flash desalination plants using radial basis function neural network, *Chemical Engineering Journal*, 162 (2010) 552-556.
- [16] N. Bhat, T.J. McAvoy, Use of neural nets for dynamic modelling and control of chemical process system, *Computers & Chemical Engineering*, 14 (1990) 573-582.
- [17] K.J. Hunt, D.Sbarbaro, R.Zbikowski, P.J. Gawthrop, Neural networks for control system – A survey, *Automatica*, 28 (1992) 1083-1112.
- [18] D.C. Psychogios, L.H. Ungar, A hybrid neural-network first principles approach to process modeling, *American Institute of Chemical Engineering Journal*, 38 (1992) 1499.
- [19] M.T. Hagan, H.B. Demuth, M.N. Beale, *Neural Network Design*. Boston, PWS Publishing Company of International Thomson Publishing Inc., 1996.
- [20] N.G. Voros, Z.B. Maroulis, D. Marinos-Kouris, Salt and water permeability in reverse osmosis membranes, *Desalination* 104 (1996) 141-154.
- [21] P.L.T. Brian, Concentration polarization in reverse osmosis desalination with variable flux and incomplete salt rejection, *Industrial and Engineering Chemistry Foundations*, 4 (1965) 439-445.

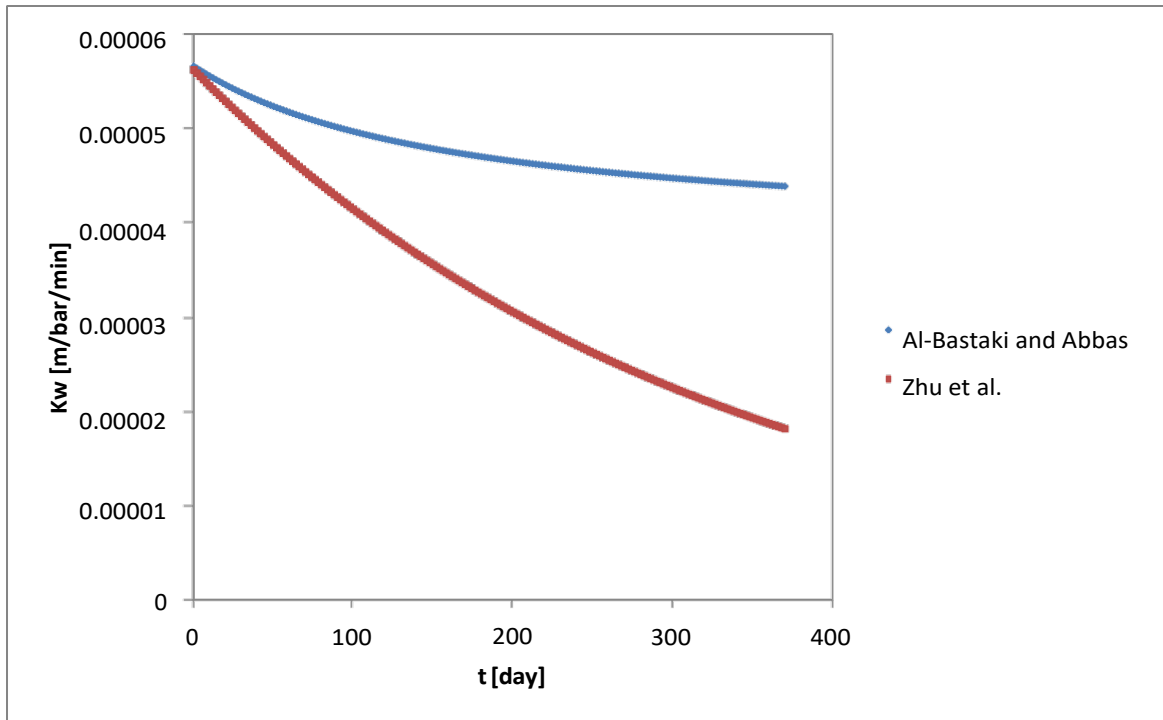


Figure 1. Water permeability trend according to literature correlations [11,15] for a period of 370 days.

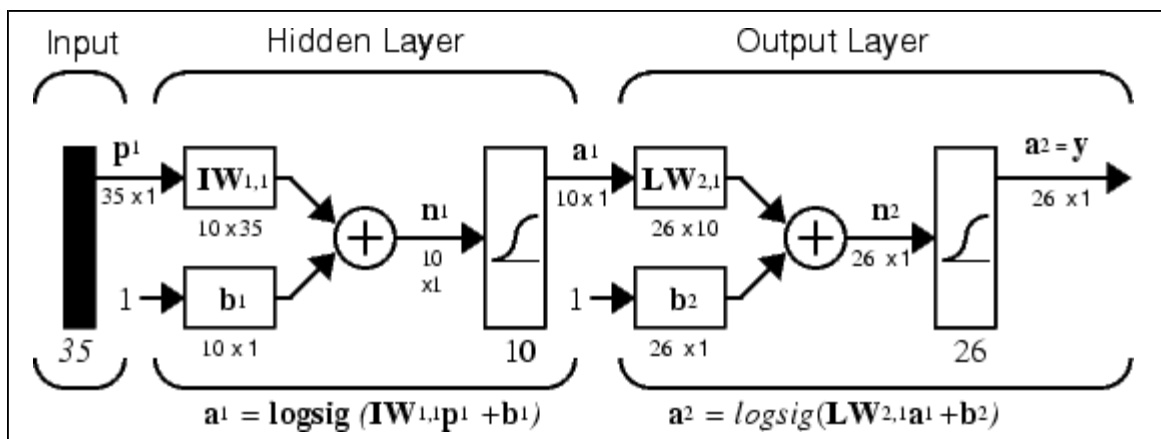


Figure 2. A typical neural network architecture (adapted from Matlab® User's guide).

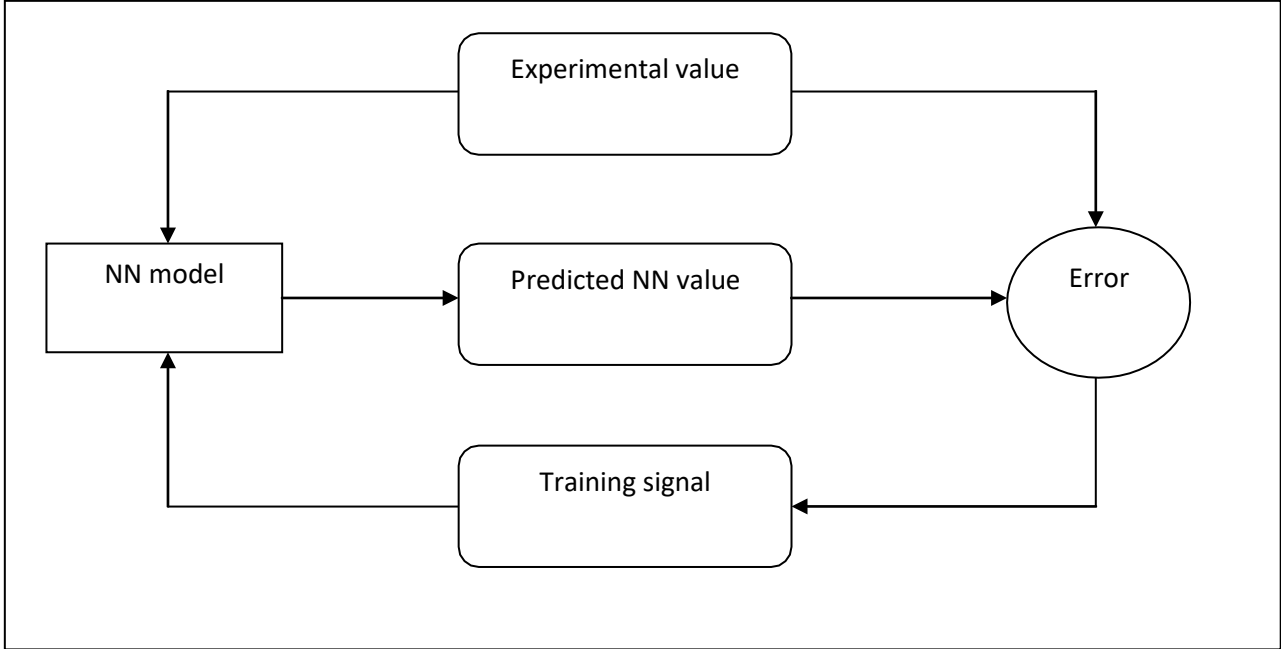


Figure 3. Back propagation algorithm scheme

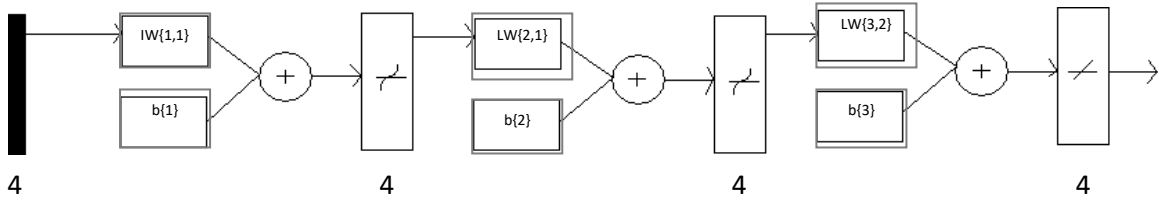


Figure 4. A three layer neural network

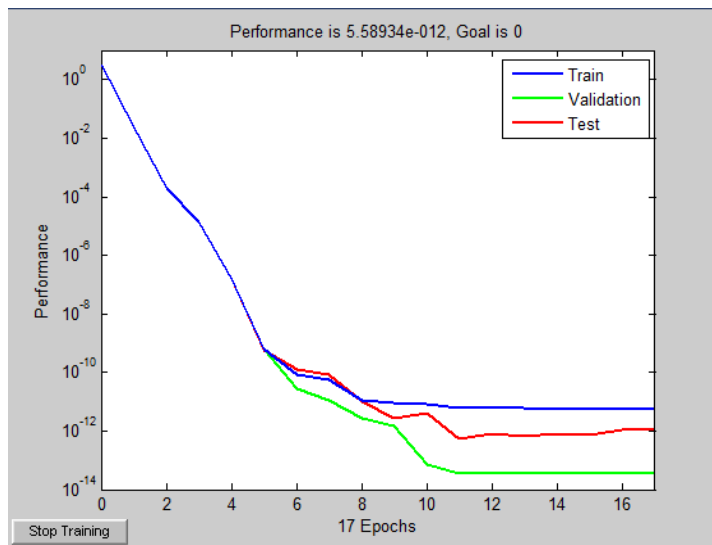


Figure 5. Performance evaluation of the NN training procedure

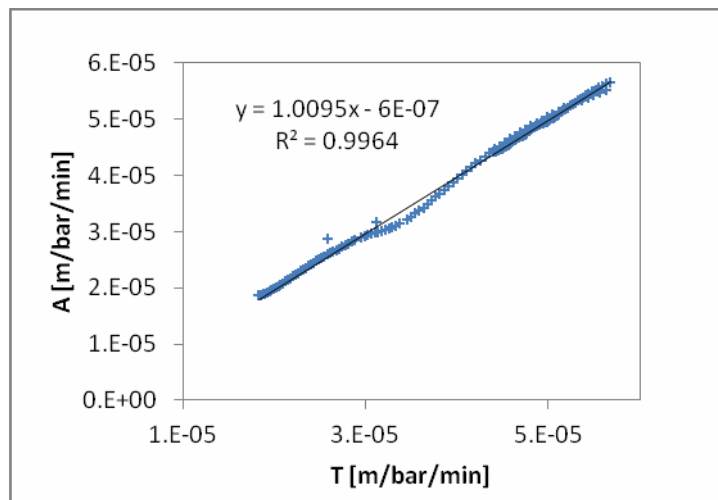


Figure 6. Linear regression of NN predicted data with correlations

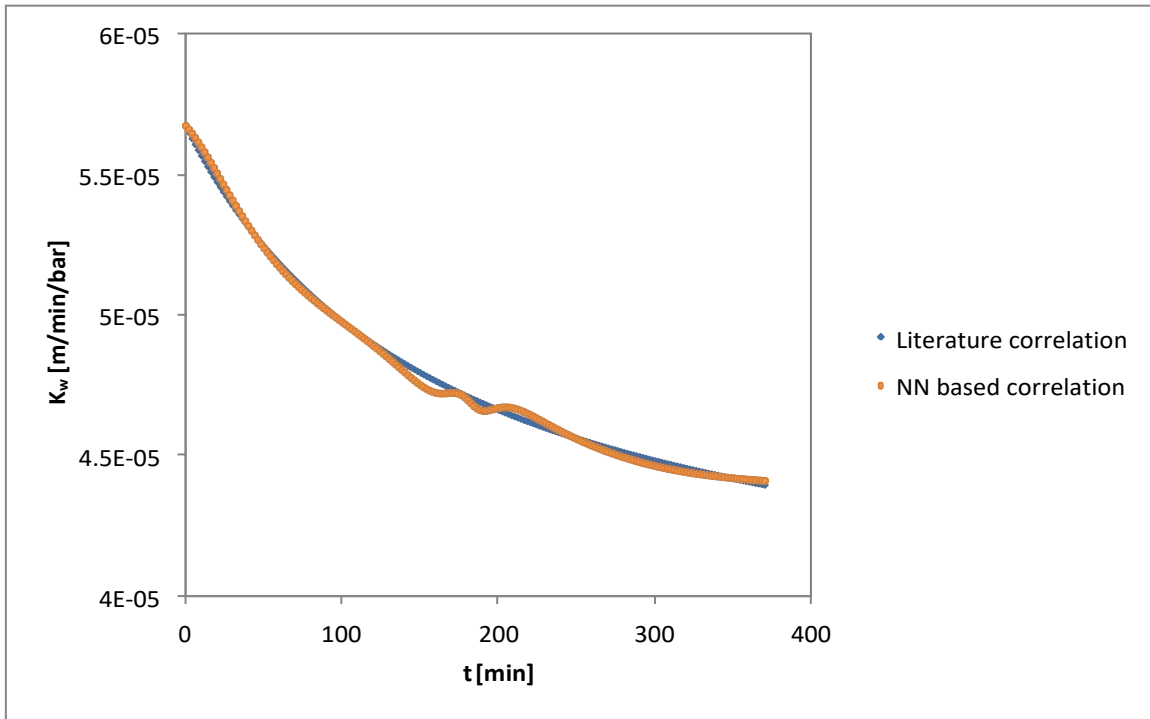


Figure 7. K_w predictions by NN based correlation and comparison with the data generated by Al-Bastaki and Abbas [15] correlation

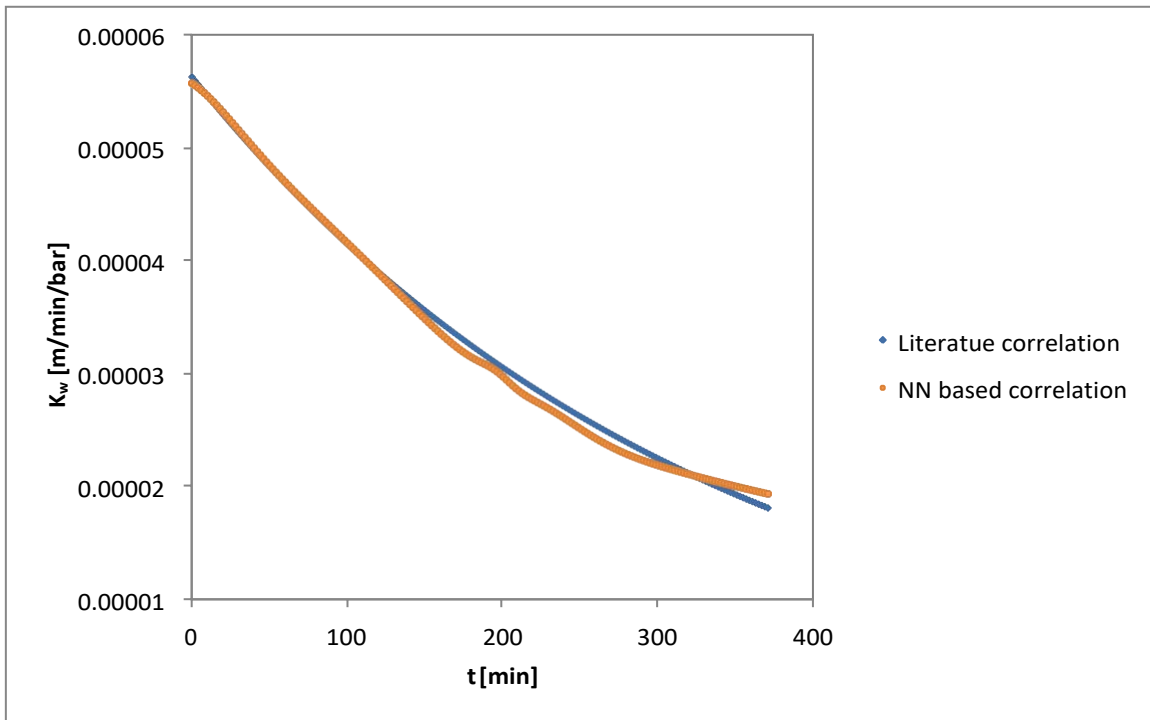


Figure 8. K_w predictions by NN based correlation and comparison with the data generated by Zhu et al. [11] correlation

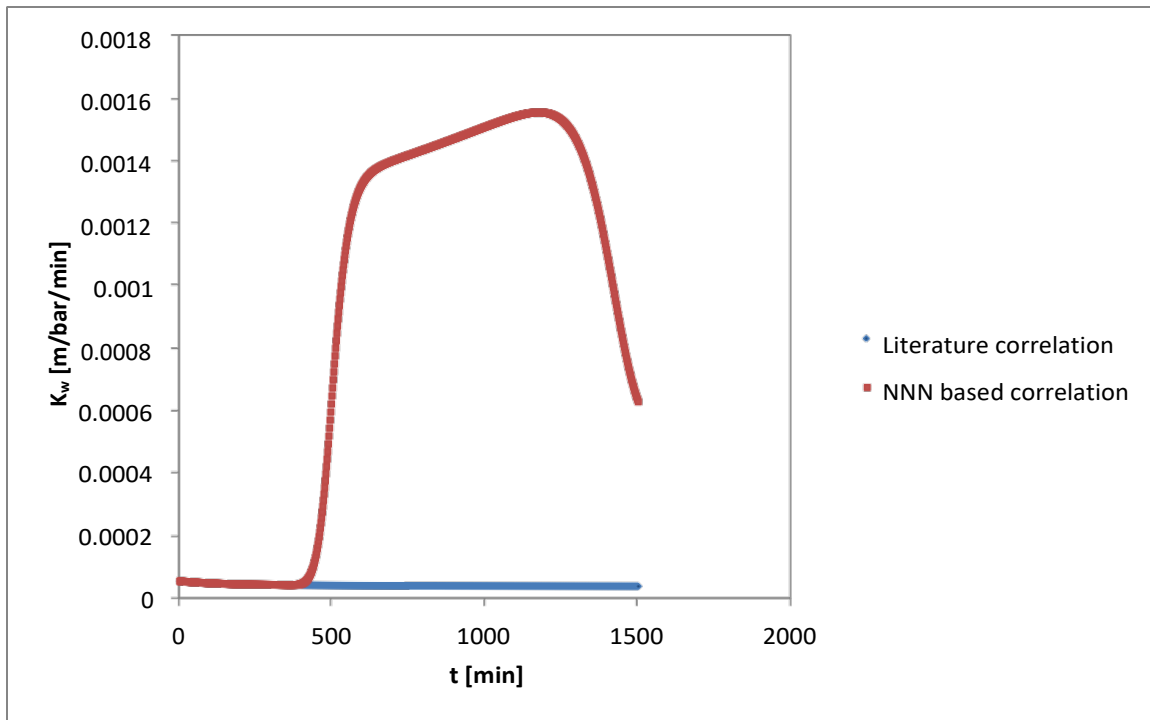


Figure 9. Zhu K_w experimental and NN based correlation extrapolation.

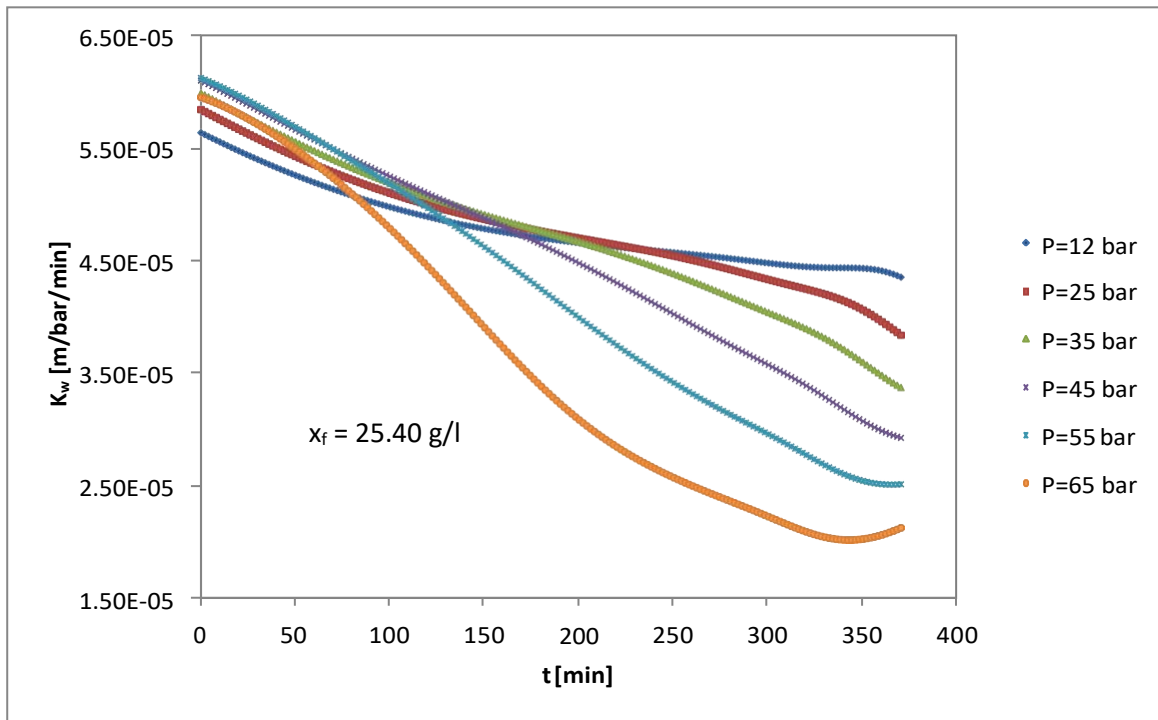


Figure 10. Water permeability constant at different pressures. [At feed salinity of Al-Bastaki and Abbas correlation]

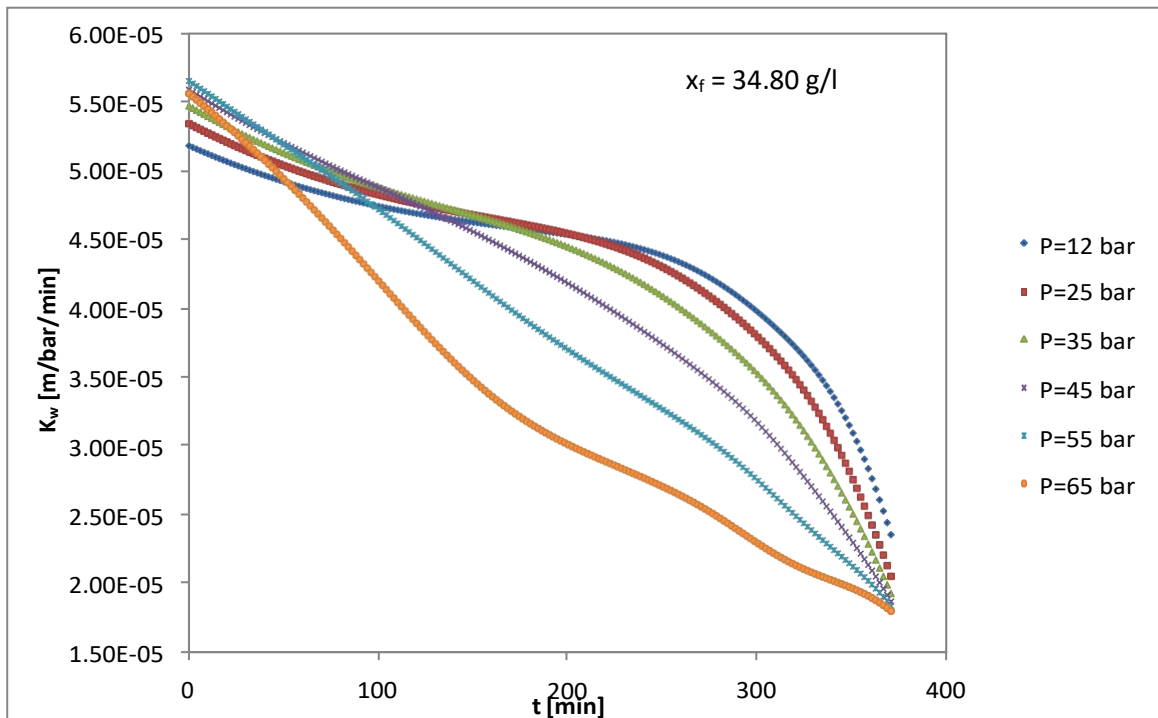


Figure 11. Water permeability constant at different pressures. [At feed salinity of Zhu *et al.* correlation]

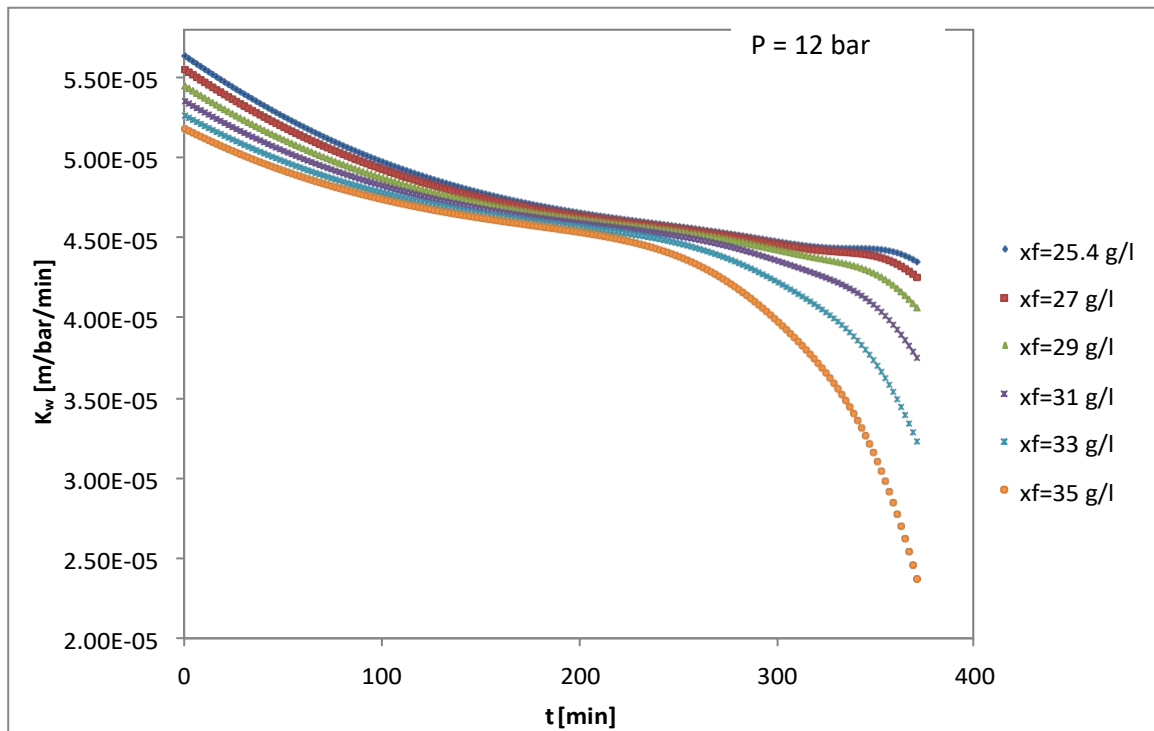


Figure 12. Water permeability constant at different feed salinity. [At pressure of Al-Bastaki and Abbas correlation]

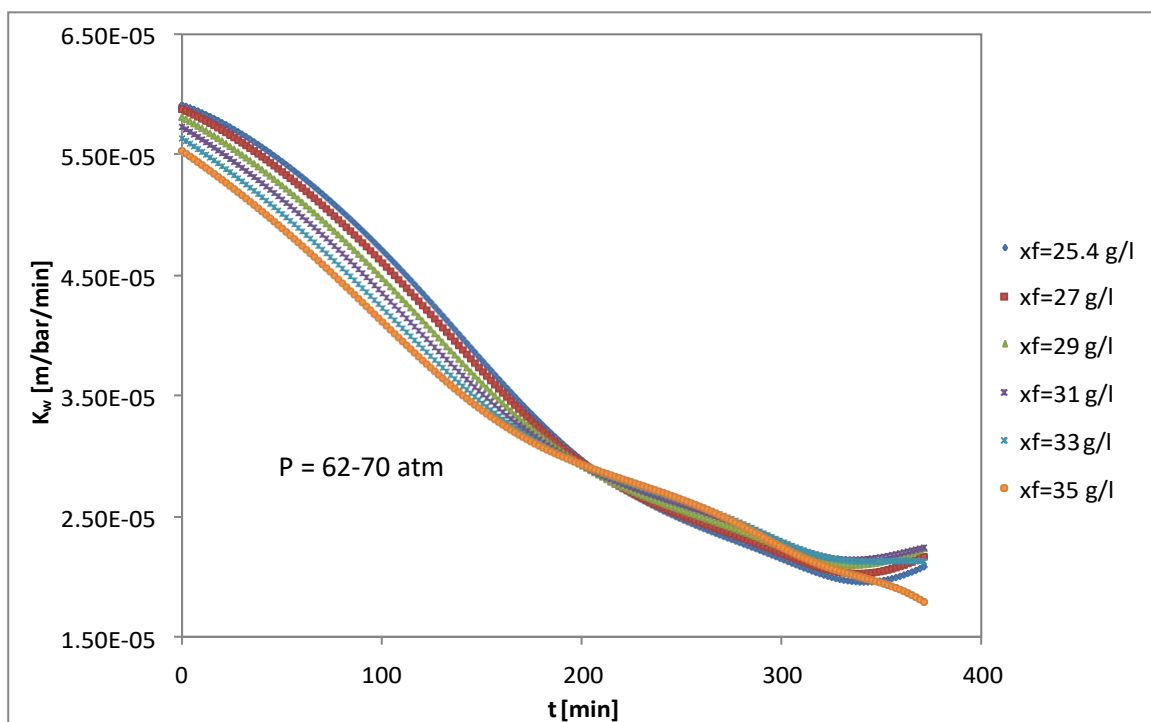


Figure 13. Water permeability constant at different feed salinity. [At pressure of Zhu *et al.* correlation]

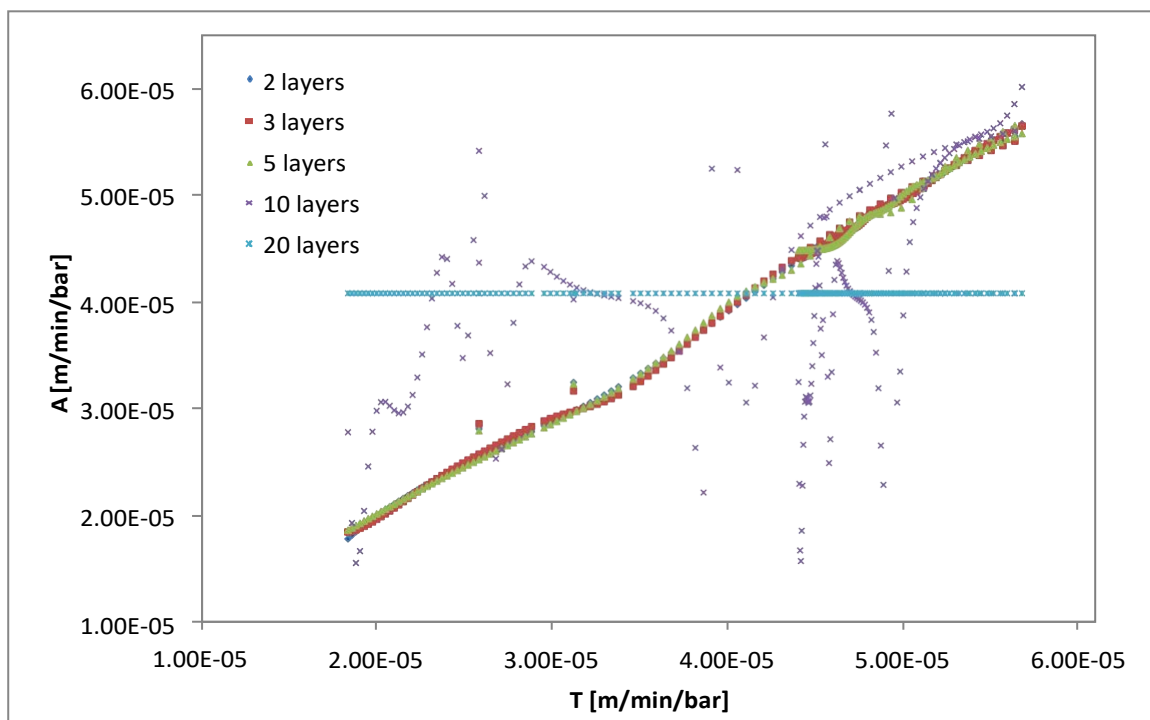


Figure 14. Effect of number of hidden layers on the NN performance.

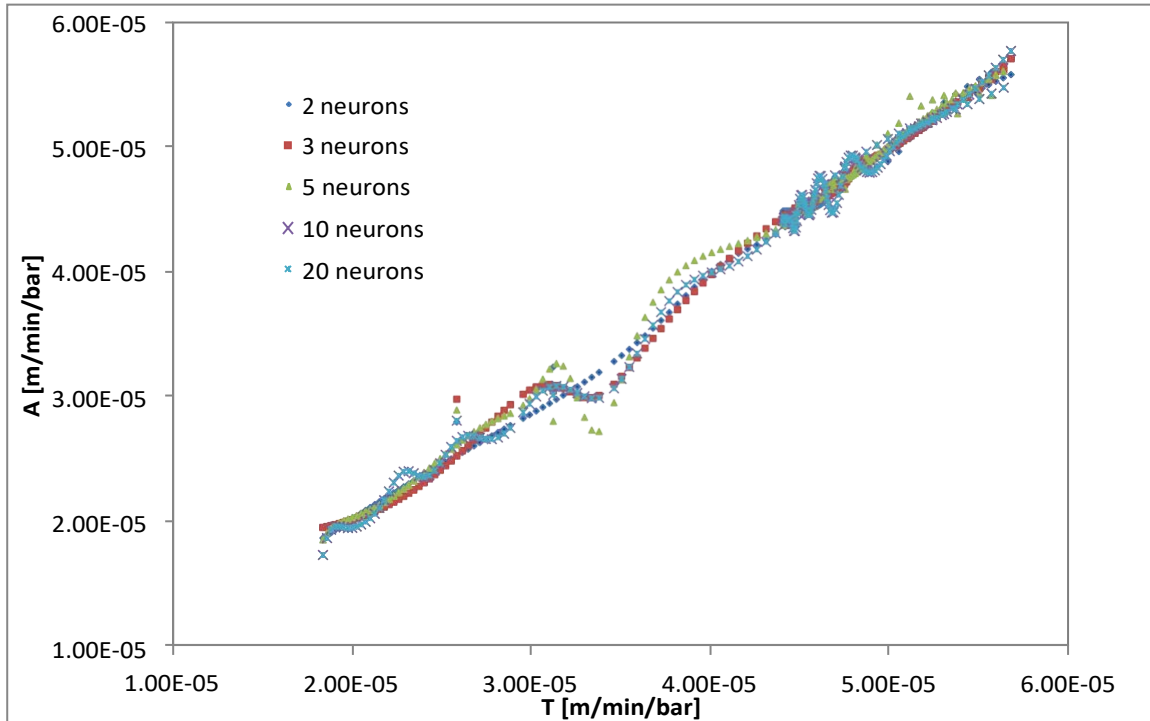


Figure 15. Effect of number of neurons on the NN performance.

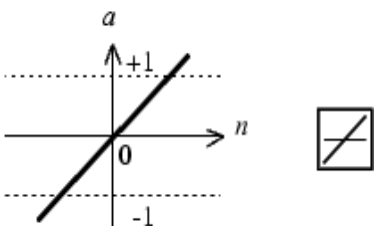
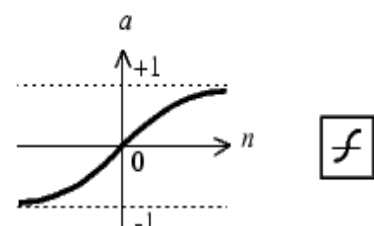
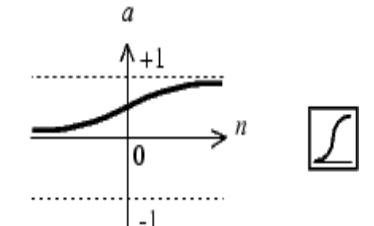
purelin	tansig	logsig
<p>Graph and Symbol</p>  <p>$a = \text{purelin}(n)$</p>	<p>Graph and Symbol</p>  <p>$a = \text{tansig}(n)$</p>	<p>Graph and Symbol</p>  <p>$a = \text{logsig}(n)$</p>

Figure 16. Transfer function list and representation.

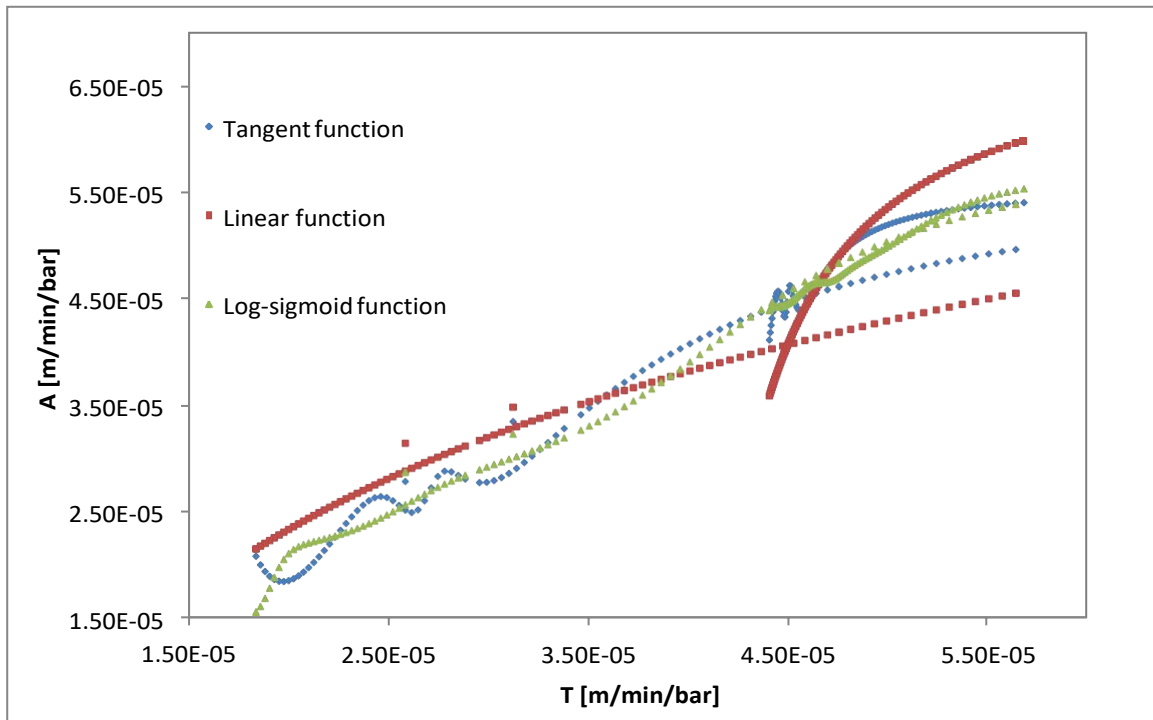


Figure 17. Transfer function influence.

Table 1.

Different correlation for estimating K_w .

Correlation 1: Al-Bastaki and Abbas [15]

$$K_w = 0.68K_w e^{\frac{79}{t+201}}$$

Membrane type: Spiral wound, Filmtec BW30-400; Feed concentration: 25.40 [g/l];

Pressure: 12 [bar]; Operating time: 1500 [d]

Correlation is based on experiments.

Correlation 2: Zhu *et al.* [11]

$$K_w = 0.68K_w e^{\frac{-t}{328}}$$

Membrane type: Hollow fiber, Dupont B-10; Feed concentration: 34.80 [g/l]

Pressure: 62-70 [atm]; Operating time: 370 [d]

Correlation is not based on experiments but is used in model-based simulation.

Table 2.

Weights, biases and transfer functions for 3-layered network.

1 st layer						
Weights				Bias	Transfer function	
w_{11}^1	w_{12}^1	w_{13}^1	w_{14}^1	b_1^1	$f_1^1 = \tanh$	
w_{21}^1	w_{22}^1	w_{23}^1	w_{24}^1	b_2^1	$f_2^1 = \tanh$	
w_{31}^1	w_{32}^1	w_{33}^1	w_{34}^1	b_3^1	$f_3^1 = \tanh$	
w_{41}^1	w_{42}^1	w_{43}^1	w_{44}^1	b_4^1	$f_4^1 = \tanh$	
2 nd layer						
Weights				Bias	Transfer function	
w_{11}^2	w_{12}^2	w_{13}^2	w_{14}^2	b_1^2	$f_1^2 = \tanh$	
w_{21}^2	w_{22}^2	w_{23}^2	w_{24}^2	b_2^2	$f_2^2 = \tanh$	
w_{31}^2	w_{32}^2	w_{33}^2	w_{34}^2	b_3^2	$f_3^2 = \tanh$	
w_{41}^2	w_{42}^2	w_{43}^2	w_{44}^2	b_4^2	$f_4^2 = \tanh$	
3 rd layer						
Weights	Bias		Transfer function			
w_{11}^3	b_1^3		$f_1^3 = 1$			
w_{21}^3						
w_{31}^3						
w_{41}^3						

Table 3.

Neural Network data (Type=1 spiral wound [15], type=2 hollow fiber [11]).

t [day]	xf [g/l]	P[bar]	Type [-]	K_w [m/bar/min]	t [day]	xf [g/l]	P[bar]	Type [-]	K_w [m/bar/min]
0	25.4	12	1	5.675E-05	186	25.4	12	1	4.698E-05
0	35	66	2	5.634E-05	186	35	66	2	3.196E-05
2	25.4	12	1	5.653E-05	188	25.4	12	1	4.694E-05
2	35	66	2	5.600E-05	188	35	66	2	3.176E-05
4	25.4	12	1	5.631E-05	190	25.4	12	1	4.689E-05
4	35	66	2	5.566E-05	190	35	66	2	3.157E-05
6	25.4	12	1	5.610E-05	192	25.4	12	1	4.684E-05
6	35	66	2	5.532E-05	192	35	66	2	3.138E-05
8	25.4	12	1	5.590E-05	194	25.4	12	1	4.679E-05
8	35	66	2	5.498E-05	194	35	66	2	3.119E-05
10	25.4	12	1	5.570E-05	196	25.4	12	1	4.674E-05
10	35	66	2	5.465E-05	196	35	66	2	3.100E-05
12	25.4	12	1	5.550E-05	198	25.4	12	1	4.670E-05
12	35	66	2	5.432E-05	198	35	66	2	3.081E-05
14	25.4	12	1	5.531E-05	200	25.4	12	1	4.665E-05
14	35	66	2	5.399E-05	200	35	66	2	3.062E-05
16	25.4	12	1	5.513E-05	202	25.4	12	1	4.661E-05
16	35	66	2	5.366E-05	202	35	66	2	3.043E-05
18	25.4	12	1	5.494E-05	204	25.4	12	1	4.656E-05
18	35	66	2	5.333E-05	204	35	66	2	3.025E-05
20	25.4	12	1	5.476E-05	206	25.4	12	1	4.652E-05
20	35	66	2	5.301E-05	206	35	66	2	3.006E-05
22	25.4	12	1	5.459E-05	208	25.4	12	1	4.647E-05
22	35	66	2	5.269E-05	208	35	66	2	2.988E-05
24	25.4	12	1	5.442E-05	210	25.4	12	1	4.643E-05
24	35	66	2	5.236E-05	210	35	66	2	2.970E-05
26	25.4	12	1	5.425E-05	212	25.4	12	1	4.639E-05
26	35	66	2	5.205E-05	212	35	66	2	2.952E-05
28	25.4	12	1	5.409E-05	214	25.4	12	1	4.634E-05
28	35	66	2	5.173E-05	214	35	66	2	2.934E-05
30	25.4	12	1	5.392E-05	216	25.4	12	1	4.630E-05
30	35	66	2	5.142E-05	216	35	66	2	2.581E-05
32	25.4	12	1	5.377E-05	218	25.4	12	1	4.626E-05
32	35	66	2	5.110E-05	218	35	66	2	2.898E-05
34	25.4	12	1	5.361E-05	220	25.4	12	1	4.622E-05
34	35	66	2	5.079E-05	220	35	66	2	2.881E-05
36	25.4	12	1	5.346E-05	222	25.4	12	1	4.618E-05
36	35	66	2	5.048E-05	222	35	66	2	2.863E-05
38	25.4	12	1	5.331E-05	224	25.4	12	1	4.614E-05
38	35	66	2	5.018E-05	224	35	66	2	2.846E-05
40	25.4	12	1	5.317E-05	226	25.4	12	1	4.610E-05

40	35	66	2	4.987E-05	226	35	66	2	2.829E-05
42	25.4	12	1	5.302E-05	228	25.4	12	1	4.606E-05
42	35	66	2	4.957E-05	228	35	66	2	2.811E-05
44	25.4	12	1	5.288E-05	230	25.4	12	1	4.602E-05
44	35	66	2	4.927E-05	230	35	66	2	2.794E-05
46	25.4	12	1	5.274E-05	232	25.4	12	1	4.598E-05
46	35	66	2	4.897E-05	232	35	66	2	2.777E-05
48	25.4	12	1	5.261E-05	234	25.4	12	1	4.594E-05
48	35	66	2	4.867E-05	234	35	66	2	2.760E-05
50	25.4	12	1	5.248E-05	236	25.4	12	1	4.590E-05
50	35	66	2	4.837E-05	236	35	66	2	2.744E-05
52	25.4	12	1	5.235E-05	238	25.4	12	1	4.586E-05
52	35	66	2	4.808E-05	238	35	66	2	2.727E-05
54	25.4	12	1	5.222E-05	240	25.4	12	1	4.583E-05
54	35	66	2	4.779E-05	240	35	66	2	2.710E-05
56	25.4	12	1	5.209E-05	242	25.4	12	1	4.579E-05
56	35	66	2	4.750E-05	242	35	66	2	2.694E-05
58	25.4	12	1	5.197E-05	244	25.4	12	1	4.575E-05
58	35	66	2	4.721E-05	244	35	66	2	2.678E-05
60	25.4	12	1	5.185E-05	246	25.4	12	1	4.572E-05
60	35	66	2	4.692E-05	246	35	66	2	2.661E-05
62	25.4	12	1	5.173E-05	248	25.4	12	1	4.568E-05
62	35	66	2	4.664E-05	248	35	66	2	2.645E-05
64	25.4	12	1	5.161E-05	250	25.4	12	1	4.564E-05
64	35	66	2	4.635E-05	250	35	66	2	2.629E-05
66	25.4	12	1	5.150E-05	252	25.4	12	1	4.561E-05
66	35	66	2	4.607E-05	252	35	66	2	2.613E-05
68	25.4	12	1	5.138E-05	254	25.4	12	1	4.557E-05
68	35	66	2	4.579E-05	254	35	66	2	2.597E-05
70	25.4	12	1	5.127E-05	256	25.4	12	1	4.554E-05
70	35	66	2	4.551E-05	256	35	66	2	2.581E-05
72	25.4	12	1	5.116E-05	258	25.4	12	1	4.550E-05
72	35	66	2	4.524E-05	258	35	66	2	2.566E-05
74	25.4	12	1	5.106E-05	260	25.4	12	1	4.547E-05
74	35	66	2	4.496E-05	260	35	66	2	2.550E-05
76	25.4	12	1	5.095E-05	262	25.4	12	1	4.544E-05
76	35	66	2	4.469E-05	262	35	66	2	2.535E-05
78	25.4	12	1	5.085E-05	264	25.4	12	1	4.540E-05
78	35	66	2	4.442E-05	264	35	66	2	2.519E-05
80	25.4	12	1	5.074E-05	266	25.4	12	1	4.537E-05
80	35	66	2	4.415E-05	266	35	66	2	2.504E-05
82	25.4	12	1	5.064E-05	268	25.4	12	1	4.534E-05
82	35	66	2	4.388E-05	268	35	66	2	2.489E-05
84	25.4	12	1	5.054E-05	270	25.4	12	1	4.531E-05
84	35	66	2	4.361E-05	270	35	66	2	2.474E-05
86	25.4	12	1	5.045E-05	272	25.4	12	1	4.527E-05

86	35	66	2	4.335E-05	272	35	66	2	2.458E-05
88	25.4	12	1	5.035E-05	274	25.4	12	1	4.524E-05
88	35	66	2	4.308E-05	274	35	66	2	2.444E-05
90	25.4	12	1	5.026E-05	276	25.4	12	1	4.521E-05
90	35	66	2	4.282E-05	276	35	66	2	2.429E-05
92	25.4	12	1	5.016E-05	278	25.4	12	1	4.518E-05
92	35	66	2	4.256E-05	278	35	66	2	2.414E-05
94	25.4	12	1	5.007E-05	280	25.4	12	1	4.515E-05
94	35	66	2	4.230E-05	280	35	66	2	2.399E-05
96	25.4	12	1	4.998E-05	282	25.4	12	1	4.512E-05
96	35	66	2	4.204E-05	282	35	66	2	2.385E-05
98	25.4	12	1	4.989E-05	284	25.4	12	1	4.509E-05
98	35	66	2	4.179E-05	284	35	66	2	2.370E-05
100	25.4	12	1	4.980E-05	286	25.4	12	1	4.506E-05
100	35	66	2	4.153E-05	286	35	66	2	2.356E-05
102	25.4	12	1	4.972E-05	288	25.4	12	1	4.503E-05
102	35	66	2	4.128E-05	288	35	66	2	2.341E-05
104	25.4	12	1	4.963E-05	290	25.4	12	1	4.500E-05
104	35	66	2	4.103E-05	290	35	66	2	2.327E-05
106	25.4	12	1	4.955E-05	292	25.4	12	1	4.497E-05
106	35	66	2	4.078E-05	292	35	66	2	2.313E-05
108	25.4	12	1	4.947E-05	294	25.4	12	1	4.494E-05
108	35	66	2	4.053E-05	294	35	66	2	2.299E-05
110	25.4	12	1	4.939E-05	296	25.4	12	1	4.491E-05
110	35	66	2	4.029E-05	296	35	66	2	2.285E-05
112	25.4	12	1	4.931E-05	298	25.4	12	1	4.488E-05
112	35	66	2	4.004E-05	298	35	66	2	2.271E-05
114	25.4	12	1	4.923E-05	300	25.4	12	1	4.485E-05
114	35	66	2	3.980E-05	300	35	66	2	2.257E-05
116	25.4	12	1	4.915E-05	302	25.4	12	1	4.483E-05
116	35	66	2	3.956E-05	302	35	66	2	2.244E-05
118	25.4	12	1	4.907E-05	304	25.4	12	1	4.480E-05
118	35	66	2	3.932E-05	304	35	66	2	2.230E-05
120	25.4	12	1	4.900E-05	306	25.4	12	1	4.477E-05
120	35	66	2	3.908E-05	306	35	66	2	2.216E-05
122	25.4	12	1	4.892E-05	308	25.4	12	1	4.474E-05
122	35	66	2	3.884E-05	308	35	66	2	2.203E-05
124	25.4	12	1	4.885E-05	310	25.4	12	1	4.472E-05
124	35	66	2	3.860E-05	310	35	66	2	2.190E-05
126	25.4	12	1	4.878E-05	312	25.4	12	1	4.469E-05
126	35	66	2	3.837E-05	312	35	66	2	2.176E-05
128	25.4	12	1	4.871E-05	314	25.4	12	1	4.466E-05
128	35	66	2	3.814E-05	314	35	66	2	2.163E-05
130	25.4	12	1	4.863E-05	316	25.4	12	1	4.463E-05
130	35	66	2	3.790E-05	316	35	66	2	2.150E-05
132	25.4	12	1	4.857E-05	318	25.4	12	1	4.461E-05

132	35	66	2	3.767E-05	318	35	66	2	2.137E-05
134	25.4	12	1	4.850E-05	320	25.4	12	1	4.458E-05
134	35	66	2	3.744E-05	320	35	66	2	2.124E-05
136	25.4	12	1	4.843E-05	322	25.4	12	1	4.456E-05
136	35	66	2	3.722E-05	322	35	66	2	2.111E-05
138	25.4	12	1	4.836E-05	324	25.4	12	1	4.453E-05
138	35	66	2	3.699E-05	324	35	66	2	2.098E-05
140	25.4	12	1	4.830E-05	326	25.4	12	1	4.451E-05
140	35	66	2	3.677E-05	326	35	66	2	2.085E-05
142	25.4	12	1	4.823E-05	328	25.4	12	1	4.448E-05
142	35	66	2	3.654E-05	328	35	66	2	2.073E-05
144	25.4	12	1	4.817E-05	330	25.4	12	1	4.446E-05
144	35	66	2	3.632E-05	330	35	66	2	2.060E-05
146	25.4	12	1	4.810E-05	332	25.4	12	1	4.443E-05
146	35	66	2	3.610E-05	332	35	66	2	2.048E-05
148	25.4	12	1	4.804E-05	334	25.4	12	1	4.441E-05
148	35	66	2	3.588E-05	334	35	66	2	2.035E-05
150	25.4	12	1	4.798E-05	336	25.4	12	1	4.438E-05
150	35	66	2	3.566E-05	336	35	66	2	2.023E-05
152	25.4	12	1	4.792E-05	338	25.4	12	1	4.436E-05
152	35	66	2	3.545E-05	338	35	66	2	2.010E-05
154	25.4	12	1	4.786E-05	340	25.4	12	1	4.433E-05
154	35	66	2	3.523E-05	340	35	66	2	1.998E-05
156	25.4	12	1	4.780E-05	342	25.4	12	1	4.431E-05
156	35	66	2	3.502E-05	342	35	66	2	1.986E-05
158	25.4	12	1	4.774E-05	344	25.4	12	1	4.429E-05
158	35	66	2	3.480E-05	344	35	66	2	1.974E-05
160	25.4	12	1	4.768E-05	346	25.4	12	1	4.426E-05
160	35	66	2	3.459E-05	346	35	66	2	1.962E-05
162	25.4	12	1	4.762E-05	348	25.4	12	1	4.424E-05
162	35	66	2	3.438E-05	348	35	66	2	1.950E-05
164	25.4	12	1	4.757E-05	350	25.4	12	1	4.422E-05
164	35	66	2	0.000E+00	350	35	66	2	1.938E-05
166	25.4	12	1	4.751E-05	352	25.4	12	1	4.419E-05
166	35	66	2	3.396E-05	352	35	66	2	1.926E-05
168	25.4	12	1	4.745E-05	354	25.4	12	1	4.417E-05
168	35	66	2	3.376E-05	354	35	66	2	1.915E-05
170	25.4	12	1	4.740E-05	356	25.4	12	1	4.415E-05
170	35	66	2	3.355E-05	356	35	66	2	1.903E-05
172	25.4	12	1	4.735E-05	358	25.4	12	1	4.413E-05
172	35	66	2	3.335E-05	358	35	66	2	1.891E-05
174	25.4	12	1	4.729E-05	360	25.4	12	1	4.410E-05
174	35	66	2	3.315E-05	360	35	66	2	1.880E-05
176	25.4	12	1	4.724E-05	362	25.4	12	1	4.408E-05
176	35	66	2	3.294E-05	362	35	66	2	1.869E-05
178	25.4	12	1	4.719E-05	364	25.4	12	1	4.406E-05

178	35	66	2	3.274E-05	364	35	66	2	1.857E-05
180	25.4	12	1	4.714E-05	366	25.4	12	1	4.404E-05
180	35	66	2	3.255E-05	366	35	66	2	1.846E-05
182	25.4	12	1	4.709E-05	368	25.4	12	1	4.402E-05
182	35	66	2	3.235E-05	368	35	66	2	1.835E-05
184	25.4	12	1	4.703E-05	370	25.4	12	1	4.399E-05
184	35	66	2	3.215E-05	370	35	66	2	1.824E-05

Table 4.
Scaled up parameters.

	MEAN	STD
<i>t</i> [min]	185.000	107.530
<i>xf</i> [g/l]	30.200	4.806
<i>P</i> [bar]	39.000	27.036
<i>Type</i> [-]	1.500	0.501
<i>K_w</i> [m/bar/min]	4.080E-05	1.100E-05

Table 5.

Calculated weights and biases of the neural network.

1 st layer					
Weights				Bias	Transfer function
$w_{11}^1 = -0.040$	$w_{12}^1 = 0.007$	$w_{13}^1 = -0.013$	$w_{14}^1 = 0.016$	$b_1^1 = 11.253$	$f_1^1 = \tanh$
$w_{21}^1 = -0.171$	$w_{22}^1 = 0.053$	$w_{23}^1 = 0.037$	$w_{24}^1 = 0.017$	$b_2^1 = -7.527$	$f_2^1 = \tanh$
$w_{31}^1 = 0.038$	$w_{32}^1 = -0.060$	$w_{33}^1 = 0.012$	$w_{34}^1 = -0.005$	$b_3^1 = 3.792$	$f_3^1 = \tanh$
$w_{41}^1 = -0.005$	$w_{42}^1 = 0.002$	$w_{43}^1 = -0.001$	$w_{44}^1 = 0.005$	$b_4^1 = -0.060$	$f_4^1 = \tanh$
2 nd layer					
Weights				Bias	Transfer function
$w_{11}^2 = 0.229$	$w_{12}^2 = 1.226$	$w_{13}^2 = -1.008$	$w_{14}^2 = 0.016$	$b_1^2 = -1.884$	$f_1^2 = \tanh$
$w_{21}^2 = -1.487$	$w_{22}^2 = 1.138$	$w_{23}^2 = -1.176$	$w_{24}^2 = 0.017$	$b_2^2 = -7.527$	$f_2^2 = \tanh$
$w_{31}^2 = 1.002$	$w_{32}^2 = 0.958$	$w_{33}^2 = -0.876$	$w_{34}^2 = -0.005$	$b_3^2 = 3.792$	$f_3^2 = \tanh$
$w_{41}^2 = -0.874$	$w_{42}^2 = 0.746$	$w_{43}^2 = -0.084$	$w_{44}^2 = 0.005$	$b_4^2 = -0.060$	$f_4^2 = \tanh$
3 rd layer					
Weights	Bias		Transfer function		
$w_{11}^3 = 1.807E - 5$	$b_1^3 = 4.823E - 5$		$f_1^3 = 1$		
$w_{21}^3 = 2.476E - 5$					
$w_{31}^3 = 3.334E - 5$					
$w_{41}^3 = -8283E - 5$					

Table 6.

Number of layers performance evaluations

	2 layers	3 layers	5 layers	10 layers	20 layers
Performance	5.96E-12	5.81E-12	5.38E-12	1.13E-10	1.25E-12
Epochs	16	26	53	19	3

Table 7.

Number of neurones performance evaluations.

	2 neurones	3 neurones	5 neurones	10 neurones	20 neurones
Performance	5.96E-12	5.67E-12	5.14E-12	5.86E-12	4.89E-12
Epochs	39	34	99	100	42

Table 8.

Performance of the NN training procedure as a function of the adopted transfer functions.

	purelin	tansig	logsig
Performance	2.29E-11	5.17E-12	5.97E-12
Epochs	5	60	58